

Structural and electronic properties of boron-induced defects on the Si(001) surfaceDaejin Eom^{✉,*}, Chang-Youn Moon,[†] and Ja-Yong Koo[‡]*Korea Research Institute of Standards and Science, Yuseong, Daejeon 34113, Republic of Korea*

(Received 11 July 2019; revised manuscript received 22 August 2019; published 4 October 2019)

The (001) surface of heavily boron (B) doped silicon is investigated by employing the scanning tunneling microscopy measurements and the density functional theory calculations. Two different defect structures are found in the surface layers, both of which evolve the characteristic spectral features near the valence band maximum. One of the two incorporates a B atom in the second layer with the Si dimers intact and is scattered randomly in the layer. The other one incorporates a B atom in the fourth layer with a dimer vacancy produced directly above it and tends to get together with nearby dimer vacancies to grow the extended or line defects along the perpendicular direction to the dimer rows. Such defect formation is energetically favored to enhance the B populations in the second and fourth layers by ~ 120 and ~ 80 times, respectively, when compared to that in the bulk layer.

DOI: [10.1103/PhysRevB.100.165301](https://doi.org/10.1103/PhysRevB.100.165301)

Boron (B) is a major *p*-type dopant in silicon (Si) and has been studied extensively for decades. As the sizes of electronic devices shrink down to the nanometer scales, ultradense B atoms near the Si surface become of particular importance because it is indispensable to exploit the surface channel with high dopant concentrations near the surface region to cope with the short channel effects. It is already well established that the δ layer of the B atoms is formed in the subsurface of Si(111) when this surface becomes B-rich by, e.g., implanting the B atoms onto the Si(111) surface [1], thermally decomposing decaborane ($B_{10}H_{14}$) molecules on the clean Si(111)- 7×7 surface [2], sputtering a solid B target onto the clean Si(111)- 7×7 surface, or simply annealing heavily B-doped Si(111) wafers [3]. In this δ layer, the B atoms substitute one third of the Si atoms to yield the $\sqrt{3} \times \sqrt{3}$ surface structure and generate the surface or resonance states far above the conduction band minimum (CBM) and far below the valence band maximum (VBM) but not in the Si band gap [1–3].

On the other hand, the B-induced structures in the Si(001) surface as well as their electronic characteristics are not resolved as comprehensively as those in the Si(111) surface even though most Si-based electronic devices are fabricated with the Si(001) wafer. Early studies measured the efficiency of B atoms as a *p*-type dopant in the Si(001) surface [4] and suggested the possible ordered state of B atoms up to 0.5 monolayer (ML) of B coverage in the subsurface layer of Si(001) [5]. A study by scanning tunneling microscopy (STM) on the B-rich Si(001) surface proposed the atomic structure of B-induced $c(4 \times 4)$ with 0.5 ML of B coverage in the second layer of Si(001) [6]. The samples in this study were prepared by exposing the clean Si(001) surface to 1% diborane (B_2H_6) in He (5000 Langmuir) or purified decaborane molecules followed by annealing at 1000 K for 90 s. The subsequent STM

studies, for which the samples were prepared by annealing heavily B-doped Si(001) wafers at ~ 1450 K, reported the paired protrusion features on the Si(001) surface and proposed various atomic models with the B atoms in the third layer [7], on the surface [8], or in the second layer of Si(001) [9]. Other studies simply assumed that the B atoms were incorporated in the second layer of Si(001) [10,11]. The theoretical studies also proposed several atomic structures with the B atoms in the second layer [12–15] or in the first and third layers [16] of Si(001).

In this work, we have investigated the heavily B-doped Si(001) surfaces by employing the scanning tunneling microscopy/spectroscopy (STM/S) measurements and the density functional theory (DFT) calculations. We find two different B-incorporated structures as well as a simple dimer vacancy (DV) structure in the B-rich Si(001) surface. We also find that the two B-incorporated structures evolve the characteristic spectroscopic features near the VBM. The DFT calculations, which are in good agreement with the STM/S measurements, suggest that a B atom occupies the substitutional site in the second and fourth subsurface layer of Si(001), respectively, for the two B-incorporated structures. Especially, the latter is stabilized by generating a DV on the top surface directly above the B atom as is the carbon (C)-induced DV41 defect [17].

The experiments were performed using a low temperature STM (Unisoku USM-1300S3He) in an ultrahigh vacuum (UHV) chamber whose base pressure is below 1×10^{-10} Torr. The B-rich Si(001) surfaces are prepared by annealing heavily B-doped Si(001) wafers in the UHV chamber. This method will lower the chance of metal or C contaminations compared to other methods in which the B atoms are injected into the Si wafer from the external sources via the sputtering or chemical vapor deposition techniques. This would be critical for our study because even minor contamination on Si(001) can result in a drastic change in the surface structure. For example, the entire Si(001) surface is transformed into a $2 \times n$ structure by a mere trace of Ni contamination [18] or into

* d.eom@kriss.re.kr

† cymoon@kriss.re.kr

‡ koojayon@kriss.re.kr

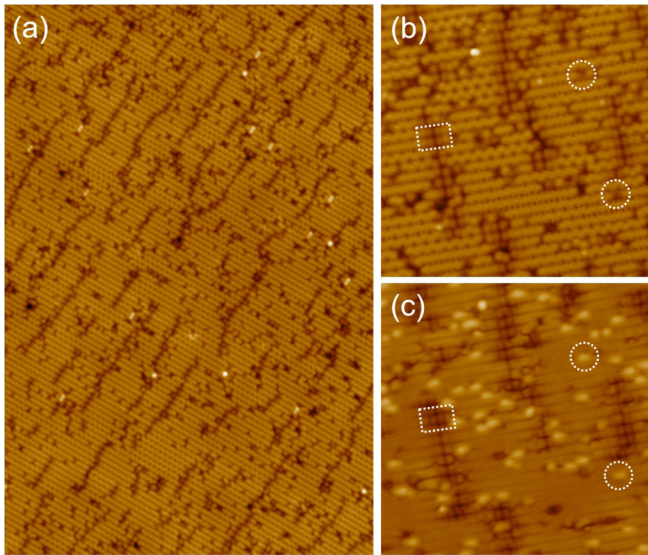


FIG. 1. STM topographies of heavily B-doped Si(001) surface, whose bulk B concentration is $\sim 8.5 \times 10^{18} \text{ cm}^{-3}$. (a) It has a lateral dimension of $53 \times 80 \text{ nm}^2$ and is imaged with the sample bias voltage $V_s = -2.0 \text{ V}$ and the tunneling current $I_t = 0.3 \text{ nA}$. (b) and (c) STM topographies taken over the same region with the lateral dimension of $20 \times 20 \text{ nm}^2$. Their imaging parameters are (b) $V_s = -2.0 \text{ V}$ and $I_t = 0.3 \text{ nA}$, and (c) $V_s = +1.5 \text{ V}$ and $I_t = 0.3 \text{ nA}$, respectively. The dotted circle and rectangle indicate two different types of B-induced defects.

a $c(4 \times 4)$ structure by a small amount of C contamination [19]. The bulk B concentrations of our samples are either $\sim 8.5 \times 10^{18} \text{ cm}^{-3}$ or $\sim 1.7 \times 10^{20} \text{ cm}^{-3}$. The native oxides of our samples are removed by the repeated thermal flashes up to $\sim 1400 \text{ K}$ in the UHV chamber. After the last flash, the samples are annealed at $\sim 600 \text{ K}$ for hours and then cooled down to the room temperature (RT) rather slowly, that is, at the rate of $\sim 2 \text{ K/sec}$. These thermal cycles are already proven to give the characteristic $\sqrt{3} \times \sqrt{3}$ structure over the wide surface area with very low defect density as well as with negligible contamination when applied to heavily B-doped Si(111) surfaces [20]. After the thermal annealing procedure, our Si(001) wafers are transferred to the STM stage and are cooled down to $\sim 80 \text{ K}$ for the STM/S measurements.

Figure 1(a) is a typical filled-state STM image of the Si(001) surface, whose bulk B concentration is $\sim 8.5 \times 10^{18} \text{ cm}^{-3}$. It shows two types of point defects; one forms line defects extended along the perpendicular direction to the Si dimer rows, and the other is isolated from each other and scattered over the surface. Figures 1(b) and 1(c) are the filled- and empty-state STM images, respectively, which are taken over the same surface area but in a different region from that in Fig. 1(a). They reveal that the line defects appear as the dark features in both images whereas the isolated ones exhibit the polarity-dependent change, i.e., from the dark features in the filled-state image to the bright ones in the empty-state one except for a few defects. The line and isolated defects also exhibit different local symmetries. That is, the latter has the asymmetric topographic feature with respect to the dimer row axis and occupies two dimer sites along the dimer row

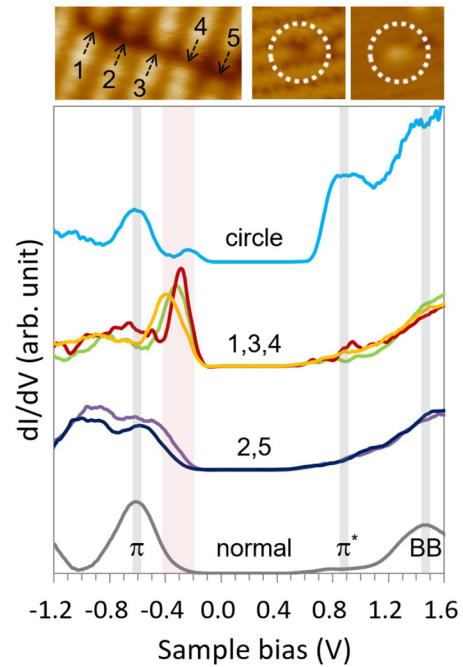


FIG. 2. dI/dV spectra taken at various defect sites as well as on the normal Si(001) surface. The bottommost (topmost) curve is taken on the normal Si(001) surface (at the defect site enclosed by the circle in the upper right insets). The other curves are taken at five different positions in the upper left inset with each spectrum being labeled by the site number. The occupied and unoccupied surface states as well as the back-bond states of normal Si(001) surface are indicated by the symbols π , π^* , and BB, respectively.

direction [see the dotted circle in Figs. 1(b) and 1(c)], being similar to the randomly scattered type-C defects produced by the dissociative adsorption of H_2O molecules on the Si(001)- 2×1 surface [21]. Whereas the former shows one DV and two neighboring depressed Si dimers on both sides along the dimer row direction and has the mirror symmetries with respect to both dimer and dimer row axes [see the dotted rectangle in Figs. 1(b) and 1(c)]. It resembles the C-induced DV41 defect on the Si(001)- 2×1 surface for which a Si dimer is vacant to accommodate a C atom directly below it and its neighboring two Si dimers along the dimer row direction becomes depressed in both filled- and empty-state STM images [17]. The C-induced DV41 defects also tend to align with other DV-type defects in the perpendicular direction to the Si dimer rows as do the line defects in Fig. 1. However, the symmetric line defects in Fig. 1 exhibit dissimilar electronic properties from the C-induced DV41 defect as is discussed shortly. On the other hand, the paired protrusion features reported in the previous STM studies on the heavily B-doped Si(001) surfaces [7–9] are rarely observed in this study. We ascribe it to the difference in the sample annealing condition or procedure between this and previous studies.

The electronic properties of symmetric line and asymmetric isolated defects in Fig. 1 are probed by using the STS technique. Figure 2 displays the differential conductance (dI/dV) spectra measured at five different positions along the line defect in the upper left inset as well as at the isolated defect enclosed by the circle in the upper right insets. The dI/dV

spectrum measured at the normal surface is also included in Fig. 2 for a comparison. The dI/dV curves taken at the line defect show two distinct spectra, one taken at the positions 1, 3, and 4 and the other at the positions 2 and 5. The former evolves a strong peak feature near the VBM or π -band edge of the Si(001) surface whereas the latter has a similar structure to that of the normal surface without showing any peak feature near the VBM. In fact the point defect at positions 2 and 5 has the characteristic topographic feature of asymmetric 2-DV defect [22] (or type-B defect [23]), which consists of two successive DVs with one of the two neighboring Si dimers depressed downward. It evolves the similar energy spectrum as that of the normal Si(001) surface with a slight change of the density of states in the rather deep valence band, as the dI/dV spectra at positions 2 and 5 do, because newly produced four dangling bonds of each DV make two Si-Si bonds. This 2-DV defect is found abundantly on the strained Ni-contaminated Si(001)- $2 \times n$ surface and also found not rarely even on the clean Si(001)- 2×1 surface [18,23]. The dI/dV curve taken at the isolated defect also evolves a spectral feature near the VBM or π -band edge of the Si(001) surface as the positions 1, 3, and 4 of the line defect do. But its intensity is rather weak compared to the latter one. Instead, it evolves another strong peak in the π^* band. Thus, the B-related defect sites in Fig. 1 are divided into two categories: (1) the isolated, asymmetric one with the spectral peak feature near the VBM, (2) the symmetrically depressed one in the line defects which evolves the spectral peak feature near the VBM.

Now we employ the DFT calculations to find the proper defect structures for the above two categories. Our first principles calculations are based on the density functional theory with the PAW potential [24,25] as implemented in the VASP code [26,27]. Electronic wave functions are expanded with plane waves up to a cutoff energy of 318 eV. A slab structure of 11 Si ML thick (16 Å) containing $c(8 \times 8)$ units of the Si(001) surface structure is constructed to mimic the Si(001) surface with reduced intercell interaction, where the dangling bonds on the bottom Si layer are passivated by hydrogen atoms. A vacuum region of about 7 Å separates the slab and its periodic images along the surface normal direction. The slab structure is taken from the bulk Si structure with the experimental lattice constant and then fully relaxed, except for the hydrogen atoms and Si atoms on the bottom layer representing the rigidity of the bulk region. The K-point sampling is performed on a $2 \times 2 \times 1$ Monkhorst-Pack grid [28].

We calculate the formation energies of B-incorporated structures at the Si(001)- 2×1 surface with and without the DV formation on the topmost surface as illustrated in Figs. 3(a) and 3(b), respectively, whose results are displayed in Fig. 3(c). If a Si DV is generated on the topmost surface, the subsequent B incorporation has the lowest formation energy when a B atom substitutes a Si atom in the fourth layer [i.e., site 4 in Fig. 3(a)] directly below the DV as the black line in Fig. 3(c) shows. This B-incorporated structure in the fourth layer is symmetric with respect to both the dimer and dimer row axes as is the line defect in Fig. 1(b) (see the dotted rectangle in the figure). Indeed, this is the same structure as the C-induced DV41 defect on the Si(001)- 2×1 surface except that a B atom replaces the C atom in our case [17]. We

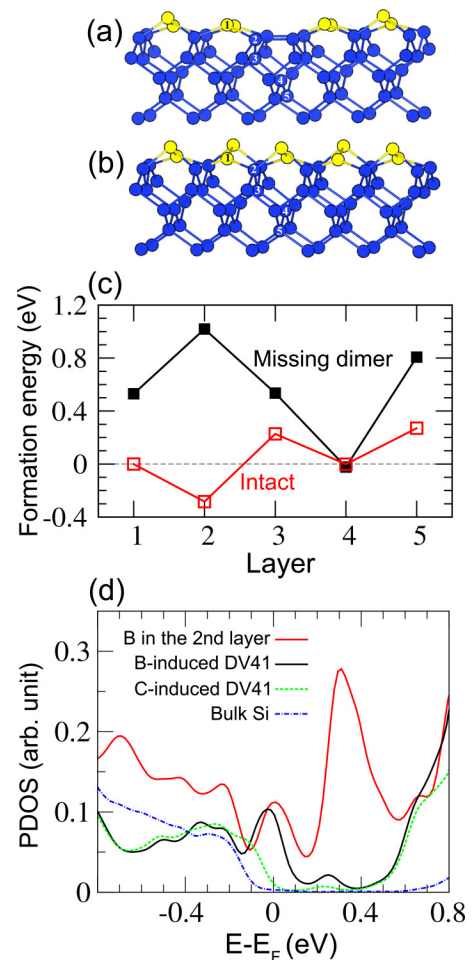


FIG. 3. (a) Atomic structure of Si dimer row with a missing dimer on the Si(001) surface where the yellow circles are the surface Si atoms. The numbers 1–5 represent the positions where a B atom can be incorporated. (b) Atomic structure of Si dimer row with all the dimers intact. (c) The calculated formation energies for the structures of (a) and (b) with a B atom occupying the position indicated by the numbers 1–5. Here the formation energy of the B incorporation into position 1 in (b) is set to zero. (d) Calculated PDOSs on surface Si atoms in the two lowest energy structures of (c), the C-induced DV41, and also on a Si atom in the bulk region.

will term this structure as the B-induced DV41 defect. If the Si(001) surface maintains its perfect 2×1 structure without the DV formation, then the B incorporation into it has the lowest formation energy when a B atom substitutes a Si atom in the second layer [i.e., site 2 in Fig. 3(b)] as the red line in Fig. 3(c) shows. This structure is asymmetric with respect to the dimer row axis as is the isolated defect in Fig. 1(b) (see the dotted circles in the figure). We will term this structure as the second-layer B defect.

The projected density of states (PDOS) of these two structures (i.e., B-induced DV41 and second-layer B defects) are also calculated in Fig. 3(d). The former one (black curve) evolves a strong peak near the VBM as do the 1,3,4 curves in Fig. 2, which belong to category 2. The latter one (red curve) also evolves a peak structure near the VBM with a slight shift toward the positive energy direction compared to the former

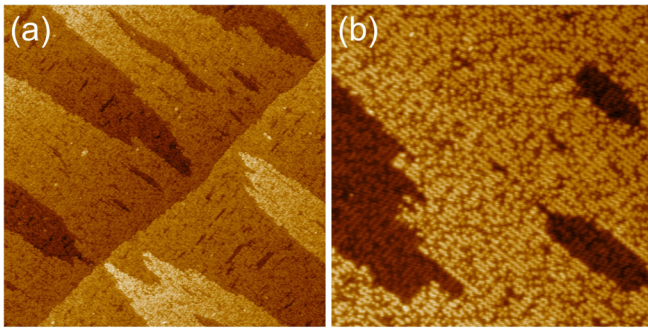


FIG. 4. STM topographies of degenerately B-doped Si(001) surface, whose bulk B concentration is $\sim 1.7 \times 10^{20} \text{ cm}^{-3}$. They are imaged with $V_s = -2.5 \text{ V}$ and $I_t = 0.3 \text{ nA}$ and have the lateral dimension of (a) $200 \times 200 \text{ nm}^2$ and (b) $50 \times 50 \text{ nm}^2$, respectively. With much more defects, the surface crystallinity is much destroyed. There is no B-induced $c(4 \times 4)$ reconstruction on the heavily B-doped surface.

one. In addition, it evolves a very pronounced peak near the CBM though this peak is rather too close to the weaker one near the VBM when compared to the blue curve in Fig. 2 because the band gap is normally underestimated in the DFT calculations. These spectral features are consistent with those of the blue curve in Fig. 2, which belongs to category 1. In short, the DFT calculations are in good agreement with the STM/S measurements in both geometric and electronic aspects for categories 1 and 2. Hence we conclude that the asymmetric isolated point defects in Fig. 1 (category 1) have the second-layer B structure with a B atom occupying site 2 in Fig. 3(b). Also we conclude that the symmetric defect sites of the line defects in Fig. 1 with the strong spectroscopic feature near the VBM (category 2) have the B-induced DV41 structure with a B atom occupying site 4 in Fig. 3(a). Noteworthy is that the B atom in the two defect structures is responsible for the characteristic peak features near the VBM in Fig. 3, which do not evolve in the C-induced DV41 defect [Fig. 3(d)].

Since the bulk B concentration in Fig. 1 is $\sim 8.5 \times 10^{18} \text{ cm}^{-3}$, its areal B density in each (001) layer is $\sim 1.2 \times 10^{11} \text{ cm}^{-2}$, that is, there is one B atom per every 5900 Si atoms in the bulk (001) layer, whose ratio is 1.7×10^{-4} . However, the number of B-induced DV41 defects (second-layer B defects) in Fig. 1 is ~ 1.4 (~ 2.1) percent of the fourth (second) layer Si atoms, implying that the B population in the fourth (second) layer is ~ 80 (~ 120) times that in the bulk layer. Such large enhancement of B populations in the surface layers relative to that in the bulk layer would build up significant p -type dopants and strains in the surface region.

Figure 4 shows the filled-state STM images of the Si(001) surface, whose bulk B concentration is $\sim 1.7 \times 10^{20} \text{ cm}^{-3}$. This doping level is ~ 20 times larger than that in Fig. 1, causing its topography to change drastically from Fig. 1: The edge of the S_B step [29] becomes rougher, the crystallinity of the dimer rows are much destroyed, and many dark features and vacancies are created on the (001) terrace. Nonetheless, we could not observe the B-induced $c(4 \times 4)$ reconstruction up to this doping level [6].

In conclusion, we have found two types of B-induced defects in the heavily B-doped Si(001) surface, which we term as B-induced DV41 and second-layer B defects, respectively. The former consists of a DV on the topmost surface with a B atom in the fourth layer directly below the DV and tends to get together with other B-induced DV41 or DV-type defects to grow the extended or line defects along the perpendicular direction to the Si dimer rows, evolving the B-induced spectral peak near the VBM. The latter is the isolated, asymmetric defect with a B atom occupying the second layer without the DV formation. It also evolves a characteristic spectral peak near the VBM. The B populations in the second and fourth layers are enhanced by ~ 120 and ~ 80 times, respectively, when compared to that in the bulk (001) layer.

This work was supported by the Basic R&D program of the Korea Research Institute of Standards and Science and partly by the Basic Science Research Program through the National Research Foundation of Korea (NRF) funded by the Ministry of Science and ICT (2016R1C1B1014715).

-
- [1] R. L. Headrick, I. K. Robinson, E. Vlieg, and L. C. Feldman, *Phys. Rev. Lett.* **63**, 1253 (1989).
 - [2] I.-W. Lyo, E. Kaxiras, and Ph. Avouris, *Phys. Rev. Lett.* **63**, 1261 (1989).
 - [3] P. Bedrossian, R. D. Meade, K. Mortensen, D. M. Chen, J. A. Golovchenko, and D. Vanderbilt, *Phys. Rev. Lett.* **63**, 1257 (1989).
 - [4] M. L. Yu, D. J. Vitkavage, and B. S. Meyerson, *J. Appl. Phys.* **59**, 4032 (1986).
 - [5] B. E. Weir, R. L. Headrick, Q. Shen, L. C. Feldman, M. S. Hybertsen, M. Needels, M. Schlüter, and T. R. Hart, *Phys. Rev. B* **46**, 12861 (1992).
 - [6] Y. Wang, R. J. Hamers, and E. Kaxiras, *Phys. Rev. Lett.* **74**, 403 (1995).
 - [7] M. A. Kulakov, Z. Zhang, A. V. Zotov, B. Bullemer, and I. Eisele, *Appl. Surf. Sci.* **103**, 443 (1996).
 - [8] T. Komeda and Y. Nishioka, *Surf. Sci.* **405**, 38 (1998).
 - [9] Z. Liu, Z. Zhang, and X. Zhu, *Phys. Rev. B* **77**, 035322 (2008).
 - [10] A. Vailionis, G. Glass, P. Desjardins, D. G. Cahill, and J. E. Greene, *Phys. Rev. Lett.* **82**, 4464 (1999).
 - [11] D. Lim, M. C. Downer, J. G. Ekerdt, N. Arzate, B. S. Mendoza, V. I. Gavrilenko, and R. Q. Wu, *Phys. Rev. Lett.* **84**, 3406 (2000).
 - [12] J. Chang and M. J. Stott, *Phys. Rev. B* **53**, 13700 (1996).
 - [13] M. Ramamoorthy, E. L. Briggs, and J. Bernholc, *Phys. Rev. Lett.* **81**, 1642 (1998).
 - [14] Y. Wang and G. S. Hwang, *Surf. Sci.* **547**, L882 (2003).
 - [15] M. Çakmak, E. Mete, and Ş. Ellialtıođlu, *Surf. Sci.* **601**, 3711 (2007).
 - [16] J. Fritsch, J. B. Page, K. E. Schmidt, and G. B. Adams, *Phys. Rev. B* **57**, 9745 (1998).
 - [17] W. Kim, H. Kim, G. Lee, and J.-Y. Koo, *Phys. Rev. Lett.* **89**, 106102 (2002).

- [18] J.-Y. Koo, J.-Y. Yi, C. Hwang, D.-H. Kim, S. Lee, and D.-H. Shin, *Phys. Rev. B* **52**, 17269 (1995).
- [19] H. Kim, W. Kim, G. Lee, and J.-Y. Koo, *Phys. Rev. Lett.* **94**, 076102 (2005).
- [20] D. Eom, C.-Y. Moon, and J.-Y. Koo, *Nano Lett.* **15**, 398 (2015).
- [21] S.-Y. Yu, H. Kim, and J.-Y. Koo, *Phys. Rev. Lett.* **100**, 036107 (2008).
- [22] J. Wang, T. A. Arias, and J. D. Joannopoulos, *Phys. Rev. B* **47**, 10497 (1993).
- [23] R. J. Hamers and U. K. Köhler, *J. Vac. Sci. Technol. A* **7**, 2854 (1989).
- [24] P. E. Blöchl, *Phys. Rev. B* **50**, 17953 (1994).
- [25] G. Kresse and D. Joubert, *Phys. Rev. B* **59**, 1758 (1999).
- [26] G. Kresse and J. Furthmüller, *Comput. Mater. Sci.* **6**, 15 (1996).
- [27] G. Kresse and J. Furthmüller, *Phys. Rev. B* **54**, 11169 (1996).
- [28] H. J. Monkhorst and J. D. Pack, *Phys. Rev. B* **13**, 5188 (1976).
- [29] J.-Y. Koo, J.-Y. Yi, C. Hwang, D.-H. Kim, G. Lee, and S. Lee, *Phys. Rev. B* **57**, 8782 (1998).